Flow-field and Noise Characterization of a Controlled-Diffusion Airfoil under stall

Kalyani, S.K.; Jaiswal, P.; Rendón, Jose ; Moreau, Stéphane ; Ragni, D.

DOI
10.2514/6.2023-4052

Publication date
2023

Document Version
Final published version

Published in
AIAA AVIATION 2023 Forum

AIAA AVIATION Forum
12-16 June 2023, San Diego, CA and Online
AIAA AVIATION 2023 Forum

10.2514/6.2023-4052

Flow-field and Noise Characterization of a Controlled-Diffusion Airfoil under stall

Sidharth Krishnan Kalyani*, Prateek Jaiswal †, Jose Rendón ‡, Stéphane Moreau§ and Daniele Ragni¶

The present experimental investigation focuses on a flow-field and noise characterization of a CD airfoil experiencing large flow separation and stall. Measurements are performed to investigate the effect of Reynolds number stalling noise signature of the CD airfoil. This study includes investigation of the potential interaction of wind tunnel shear layers with the separating shear layer of the airfoil, in an effort to validate previous experimental studies performed on a similar jet width using Planar-PIV.

While a mean flow separation is observed near the leading-edge of the CD airfoil at angles of attack $\alpha_g \geq 15°$, the mean reattaches before the trailing-edge region for the case of $\alpha_g = 15°$. In contrast for $\alpha_g = 22°$ case the mean flow becomes completely separated and airfoil experiences a deep stall. For the latter, the Sound Pressure Levels are reduced and it is possibly linked to a decrease in overall velocity disturbances and attenuation of modulations in SPL linked to diffraction. More importantly, the velocity disturbances do not scale with overall extent of the separated shear layer or the boundary layer. As such, a one to one correspondence does not exist between SPL and boundary layer thickness.

I. Introduction

Aircraft fan noise has been projected to increase with the advent of Ultra High By-pass Ration (UHBR) engines, and more fundamental research is necessary to understand the mechanisms and reduce this noise source [1, 2]. Airframe noise arises mostly from the high-lift devices [3] and landing gears [4]. These high-lift devices operate under conditions where flow separation could be significant. The noise generation due to flow separation falls well inside the range of human hearing [5][6] and could be problematic. In recent times, turbomachinery blades are installed in such a way that very high loading is achieved. This poses a significant threat of localized stall regions which could arise due to a slight change in operating conditions for which the blades are designed for [7]. On the one hand, the complexity in simulating such flow conditions lies in a high cost requirement [8], since the size and resolution in the spanwise direction necessary to resolve the spanwise length of the vortices (independent acoustic sources) responsible for noise generation [9] in separated flow regimes is higher than in an attached case. On the other hand, experiments performed previously on airfoils under separation and stalling phenomena have not been able to directly compare with each other due to varying experimental conditions, such as different jet widths and test section configurations. But a common observation from these experiments has shown that the low to mid-frequency generated noise is caused by the wall-pressure fluctuations induced by the vortices in the separated shear layer [5][10][11]. However, it was observed from the experiments of Moreau et al. [11] that the low frequency part of the noise was contaminated with the oscillation of the jet shear layers (which also fall under the low frequency category), which could mean an interaction of the jet shear layer with the vortices of the separated shear in a lower relative jet width (ratio of jet width to the airfoil chord) configuration. This caused a modulation of the low frequency content of the far-field noise. This can be easily misinterpreted as airfoil self-noise, but must instead be considered as a modification of background noise sources in the presence of the airfoil. This low frequency contamination, however was not observed in another configuration with a higher relative jet width (3.8) in the same experiments of Moreau *et al.* [11], which also had different far-field noise characteristics. Moreover, these experiments characterizing airfoil stall, including that of Lacagnina *et al.*[5] on airfoil stall do not clearly validate the absence of an interaction of the separated shear layer with the wind tunnel shear.

More recently, experiments were performed at Université de Sherbrooke (UdeS) by Kalyani *et al.* [12] to characterize the flow-field around the Controlled Diffusion (CD) airfoil and investigate the effect of Reynolds number. Firstly, there

*PhD candidate, Mechanical Engineering Department, sidharth.krishnan.kalyani@usherbrooke.ca.
†Post-doctoral fellow, Mechanical Engineering Department, prateek.jaiswal@usherbrooke.ca
‡PhD student, Mechanical Engineering Department, jose.manuel.rendon.arredondo@usherbrooke.ca
§Professor, Mechanical Engineering Department, AIAA Lifetime Member, stephane.moreau@usherbrooke.ca.
¶Associate Professor, Aerodynamics, Wind Energy, Flight Performance and Propulsion Department, Member AIAA, d.ragni@tudelft.nl.

was favourable comparison in terms of C_p for the case of α_g = 15° with earlier measurements conducted in the Ecole Centrale de Lyon (ECL) wind tunnel with the same jet width, where the Laminar Separation bubble (LSB) was predicted to cover 40% of the chord. Secondly, from the C_p distribution in [12], the airfoil was expected to stall at α_g = 22°, with probably a deeper stall for the lower Reynolds number than for the higher one. Thirdly, positive convection velocities obtained from the unsteady wall pressures near the TE revealed a possibility of small vortical structures convecting over the TE, even when the airfoil is stalled. On the other hand, the only computational work for an almost separating flow condition, the α_g = 15° of the CD airfoil was a Large Eddy Simulation (LES) performed by Christophe *et al.*[13]. From iso-contours of the Q-criterion images (refer to figure 3 in [13]), a strong creation of vorticity right at the leading edge was observed, with large vortices shed from the suction side of the airfoil. Yet there were smaller vortices that remain attached to the wall and roll over the airfoil suction side and graze at the trailing edge also yielding a positive convection velocity. The flow-field at almost separating and stalling conditions are relatively new and have not been validated yet.

Hence, based on the above considerations, the main goal of this paper is to understand the characteristics of flow-field, wall-pressure statistics and far-field noise of a CD airfoil, in an effort to address multiple objectives. They are,

- Quantify the flow field over the CD airfoil placed at high angles of attack,
- Validate the findings of the previous simulation and experiments, including the extent of the LSB and the flow-field near the TE at separation and stall.

A CD airfoil is to be utilized in the current study, which sees its application in many modern turbomachinery [14] and automotive blades [15].The boundary layer diffusion on the suction side of the CD airfoil is controlled by carefully designing the camber and thickness in such a way that from the highest point of velocity (at the leading edge) up until the trailing edge, the growth of boundary layer is kept as thin as possible. This also helps control the airfoil self-noise because the diffraction of near field disturbances to noise has been shown to be proportional to the boundary layer thickness [16].

The paper is organized as follows: section II introduces the experimental methodology, including the measurement configuration and techniques to be used in this study, and the proposed measurement campaign. Section III provides mean loading, flow-field and acoustic results from the present study, which is performed on the CD airfoil placed at very high geometrical angles of attack $\alpha_g \geq 15°$. Finally, section IV brings a short discussion and conclusions of the present manuscript.

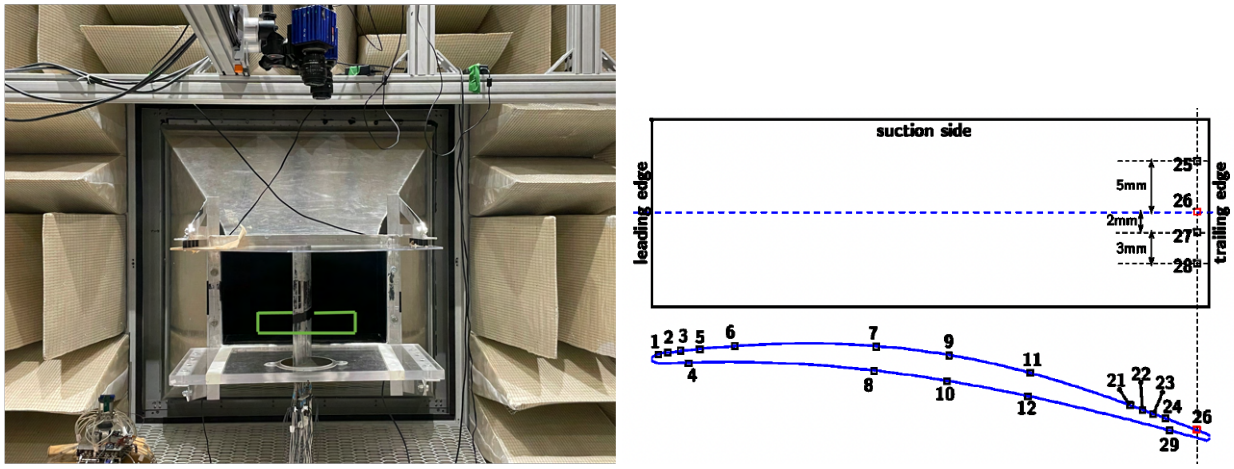

(a) **(b)**

Fig. 1 Experimental configuration at UdeS, a) the anechoic room with the nozzle exit and b) CD airfoil mock-up.

II. Experimental methodology

The experiments were performed in the UdeS anechoic wind tunnel facility [17]. The anechoic wind tunnel comprises of an anechoic room with a closed return type wind tunnel. The room dimensions are 7 x 5.5 x 4 m^3 (refer to Fig. 1a). The nozzle outlet dimensions chosen for this campaign is 50 x 30 cm^2. The turbulence intensity in the jet is reported to be below 0.4% [17], due to a strong contraction ratio of 1:25. The CD airfoil to be used has a chord (C) of 0.1345 m and a span of 0.3 m and is vertically placed between two side plates, such that the jet width is 50 cm. The

Table 1 Parameters used for the Planar PIV for two different angles of attack (α_g).

Parameters	$\alpha_g = 22°$	$\alpha_g = 15°$
Number of Images	1800	1800
Interrogation window [pixel^2]	16×16	4×4
Lenses focal Length [mm]	50	50-200
Maximum particle image displacement [pixel]	20	20

experiments are performed at two flow speeds, corresponding to 16 and 30 m/s. This is done in an effort to understand the effect of Reynolds number on the separation and stalling phenomenon on the CD airfoil. Note that these speeds allow redundancy with previous experiments run in the Ecole Centrale de Lyon anechoic wind tunnels [18].

Wall-pressure measurements were performed using pinholes (0.5 mm) already present at mid-span of the CD airfoil (Fig. 1b). The capillary tube which extends out of the blade tip is connected to a block and branches out into two; one for measuring the steady pressure, where a capillary tube is extended by a long PVC soft tube to a differential pressure measurement sensor. The second part is connected to a Knowles FG 23329 P07 electret microphone, to measure the unsteady wall pressures. The differential pressure measurement system (RCDB) used was manufactured by Neal [19] in order to measure differential pressure of a system of CD rotating blades.

Far-field acoustic pressure measurements were done using a 1/2 inch free-field PCB ICP sensor. Brüel & Kjær LAN-XI modules was utilized for acquiring the acoustics at a rate of 65536 Hz for a period of 180 seconds.

2D Planar PIV measurements were performed at two different Reynolds numbers based on chord for characterizing the flow separation and stall around the CD airfoil. A ND-YAG dual pulsed laser from Litron Inc (Nano-PIV) are used as the light source for the current investigation. A spherical doublet and a cylindrical lens, with a focal length of -10 mm, were used to generate a thin light sheet at the mid-span of the airfoil, as shown in figure 1a in green. Glycerine tracer particles of 1 μm were generated to seed the flow. For the for $\alpha_g = 22°$ case two sCMOS 5.5 Mpix cameras were used while for the for $\alpha_g = 15°$ case three sCMOS cameras were used. For $\alpha_g = 22°$, the sCMOS cameras were fitted with 50 mm lenses in order to check for the interaction of separated shear with the jet shear layers from the wind tunnel. For $\alpha_g = 15°$, three cameras are used with a combination of 50 mm for wider FOV, and 200 mm lens to focus on the LE and TE. The details of the PIV setup for both the configurations are given in table 1.

III. Results

The negative coefficient of pressure, $-C_p$, which is defined as the differential static pressure normalized by the mean free-stream dynamic pressure, is plotted as a function of airfoil chord in Figs. 2a and 2b. In these plots, $x/C = 1$ corresponds to the trailing-edge while $x/C = 0$ the leading-edge of the airfoil. Fig. 2a corresponds to $\alpha_g = 15°$ case while Fig. 2b corresponds to $\alpha_g = 22°$. As such, the mean loading on the airfoil in separation and stall is seen to be similar to that obtained in our previous experiments of Kalyani *et al.* [12] and Moreau and Roger [18]. Three data points are missing in the new measurements (UdeS 2022) because sensors 7, 8 and 9 were disconnected. A small constant offset in suction region near the LE can be attributed to a change in the atmospheric pressure or temperature in the ambient on a particular day. Regardless, there seems to be a good repeatability of previous measurements.

Since the experiments performed at UdeS have similar relative jet width (50 cm or $3.71 \times C$) as the high relative jet width case of ECL, it is expected that there is limited or no interaction of the jet shear layer with the vortices of the separated shear layer [see 20, for instance].

Fig. 3 shows mean boundary-layer statistics recorded by the first camera, for $\alpha_g = 15°$ and $U_\infty = 16$ m/s. Fig. 3 is plotted with respect to an observer sitting on the leading-edge of the airfoil. Fig. 3 shows that, in a time-averaged sense, the mean flow becomes separated from RMP 3 ($x/C = 0.09$) onward. This is consistent with Fig. 2a, which shows a plateau in C_p between RMP 3 and RMP 6. More importantly, the separated region shown by the black dashed lines in Figs. 3 has a negligible r.m.s value of velocity disturbances (all Reynolds stresses close to zero). This confirms the laminar nature of the time-averaged separated flow region, and in the literature, it is commonly referred to as the Laminar Separation Bubble (LSB). The presence of such an LSB is characteristic of the flow past the CD airfoil at $Re_c = 150000$ and is consistent with the finding of Christophe and Moreau [9], who also reported the presence of a LSB when the CD airfoil is placed at a 15° incidence.

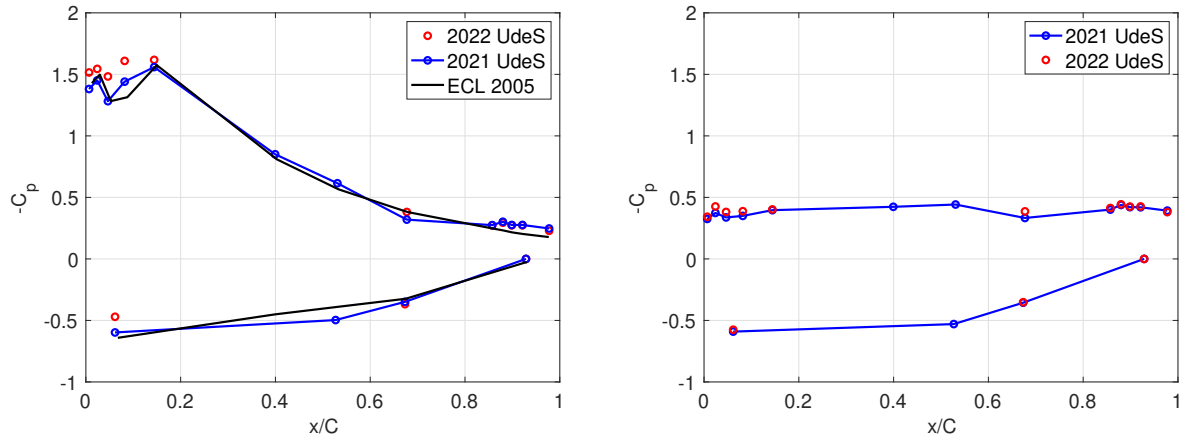

Fig. 2 Comparison of mean wall pressure data at 16m/s.

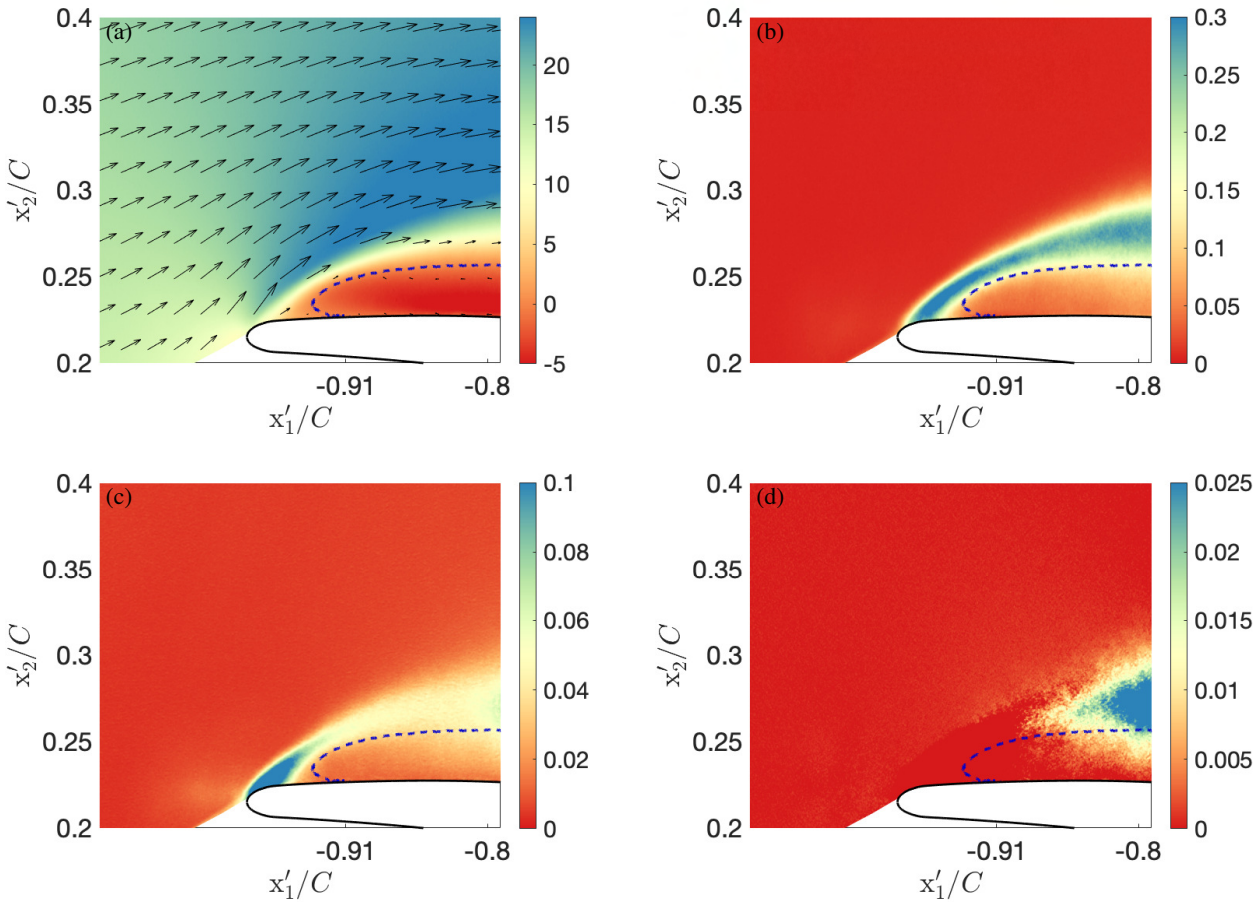

Fig. 3 Contours of velocity statistics over the airfoil leading edge (blue dashed lines are the iso-contours of zero wall-parallel velocity U_∞): (a) mean wall-parallel velocity U_1; (b) $\frac{\overline{u_1 u_1}}{U_\infty^2}$; (c) $\frac{\overline{u_2 u_2}}{U_\infty^2}$; (d) $-\frac{\overline{u_1 u_2}}{U_\infty^2}$. Coordinate system is aligned with the leading edge.

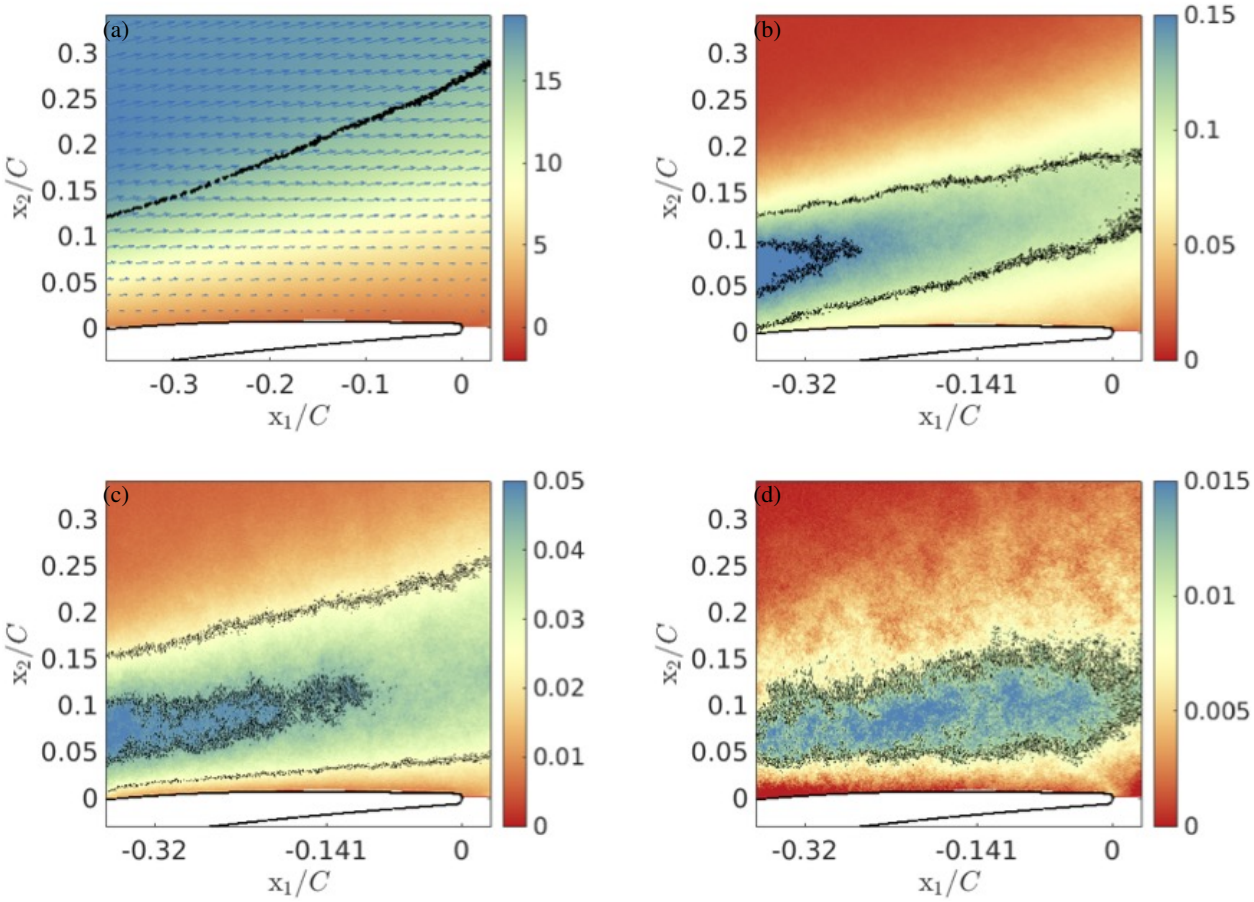

Fig. 4 Contours of velocity statistics over the airfoil trailing edge for $U_\infty = 16$ m/s and $\alpha_g = 15°$: (a) mean wall-parallel velocity U_1 (black line corresponds to free-stream inlet velocity U_∞), (b) $\frac{\overline{u_1 u_1}}{U_\infty^2}$ (black dashed lines indicate iso-values of 0.15 and 0.1); (c) $\frac{\overline{u_2 u_2}}{U_\infty^2}$, black dashed lines indicate iso-values of 0.045 and 0.025; (d) $-\frac{\overline{u_1 u_2}}{U_\infty^2}$, black dashed line indicates iso-values of 0.01. Coordinate system is aligned with the trailing edge.

The mean boundary-layer statistics recorded by the third camera are shown in Fig. 4 for the case when the airfoil is placed at a 15° angle of attack with an inlet velocity of 16 m/s. Fig. 4 (a) shows the mean wall-parallel velocity. Despite the large-scale flow separation observed in Fig. 3, the boundary-layer near the trailing edge is fully attached in a time-averaged sense. As such, in the present pre-stall noise study, the time-averaged flow near the trailing-edge of the CD airfoil is different from the one reported by Lacagnina et al. [5], who reported a separated time-averaged flow near the trailing edge. The black dotted line is the iso-contour of the inlet velocity free-stream velocity, which roughly corresponds to the overall extent of the boundary layer. The Reynolds stress tensor terms, $\overline{u_1 u_1}/U_\infty^2$, $\overline{u_2 u_2}/U_\infty^2$, and $-\overline{u_1 u_2}/U_\infty^2$, are shown in Figs. 4 (b), (c), and (d), respectively. Compared to the leading-edge region, the disturbances (quantified by r.m.s of velocities) close to the trailing-edge are substantially higher, which implies that the flow transitions to a fully turbulent boundary-layer somewhere between 40 and 65% of the chord. Higher levels of r.m.s velocities are the sources of far-field noise [21]. In particular, elevated regions of r.m.s velocity do not have a clear peak but a broad region of elevated intensity. This is typical of flows that experience the presence of shear layer instabilities [22].

In order to understand the impact of the Reynolds number, the results of the measurements performed at 28 m/s are plotted in Fig. 5. Upon comparison with figure 4, it shows similar overall behavior in the measured velocity field in the trailing-edge region. The overall length of the boundary layer is similar to the 16 m/s case at $x_2 \simeq 0.32\ C$ and close to the trailing-edge region ($x_2 \simeq 0.02\ C$). Furthermore, for the 28 m/s case, the turbulence intensity appears to be much lower than in the 16 m/s case, resulting in more localized levels of iso-contours in Fig. 5 compared to those in Fig. 4.

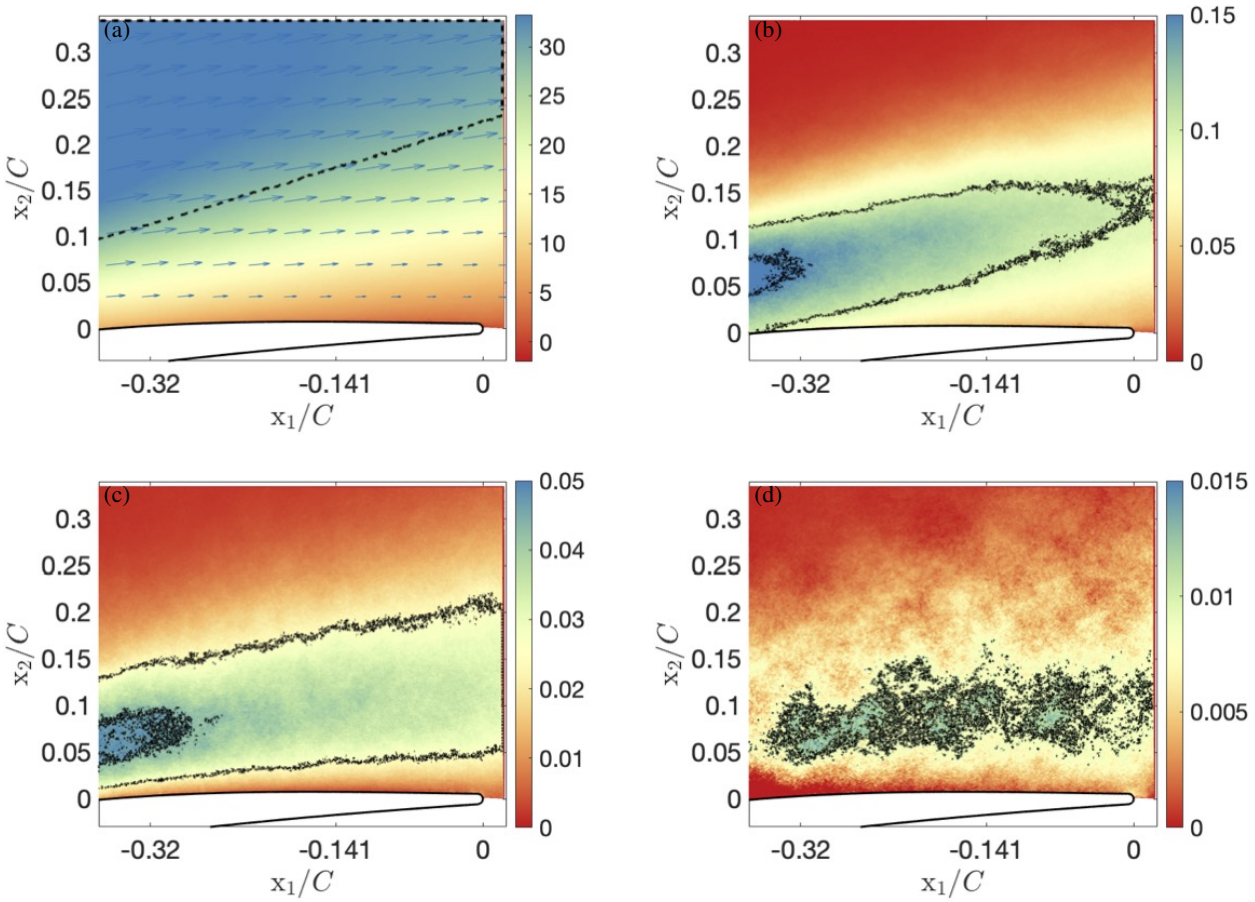

Fig. 5 Contours of velocity statistics over the airfoil trailing edge for $U_\infty = 28$ m/s and $\alpha_g = 15°$ (a) mean wall-parallel velocity U_1 (black line corresponds to free-stream inlet velocity U_∞), (b) $\frac{\overline{u_1 u_1}}{U_\infty^2}$ (black dashed lines indicate iso-values of 0.15 and 0.1); (c) $\frac{\overline{u_2 u_2}}{U_\infty^2}$, black dashed lines indicate iso-values of 0.045 and 0.025; (d) $-\frac{\overline{u_1 u_2}}{U_\infty^2}$, black dashed line indicates iso-values of 0.01. Coordinate system is aligned with the trailing edge.

Finally, to quantify the impact of changing the angle-of-attack at which the CD airfoil experiences stall [12], we show the flow-field for the CD airfoil placed at $\alpha_g = 22°$ in Fig. 6. The flow only separates at RMP 3 and onwards. Previous research [23] for an airfoil under stall have confirmed flow separation starts at the leading-edge of the airfoil. The reason for this discrepancy maybe attributed to a limited spatial resolution in the wall-normal direction. Kalyani et al. [12] performed C_p measurements at various angles of attack, and based on their results, the flow was expected to be completely separated. Nevertheless, using C_p as a metric for flow separation can sometimes be misleading. Therefore, the skin friction coefficient C_f is a more relevant parameter for detecting mean flow separation [20]. However, measurements required to estimate C_f are difficult to be employed over such as small airfoil [24, 25].

More importantly, large scale flow separation is evidenced from Fig. 6, which confirms no flow re-attachment takes places. Near the trailing-edge, at sensor RMP 26 ($x_2/C = 0.98$), the boundary-layer thickness (or separated shear layer thickness) is close to $0.83\,C$. As such, the boundary layer thickness is an order of magnitude higher than for cases when the CD airfoil is placed at a lower angle of attacks, e.g. $\alpha_g = 15°$ in Fig. 5. Yet the flow disturbances, in particular $\frac{\overline{u_2 u_2}}{U_\infty^2}$, do not scale with the boundary layer or shear layer thickness. Modal decomposition of the velocity disturbance field is performed in order to identify dominant flow structures.

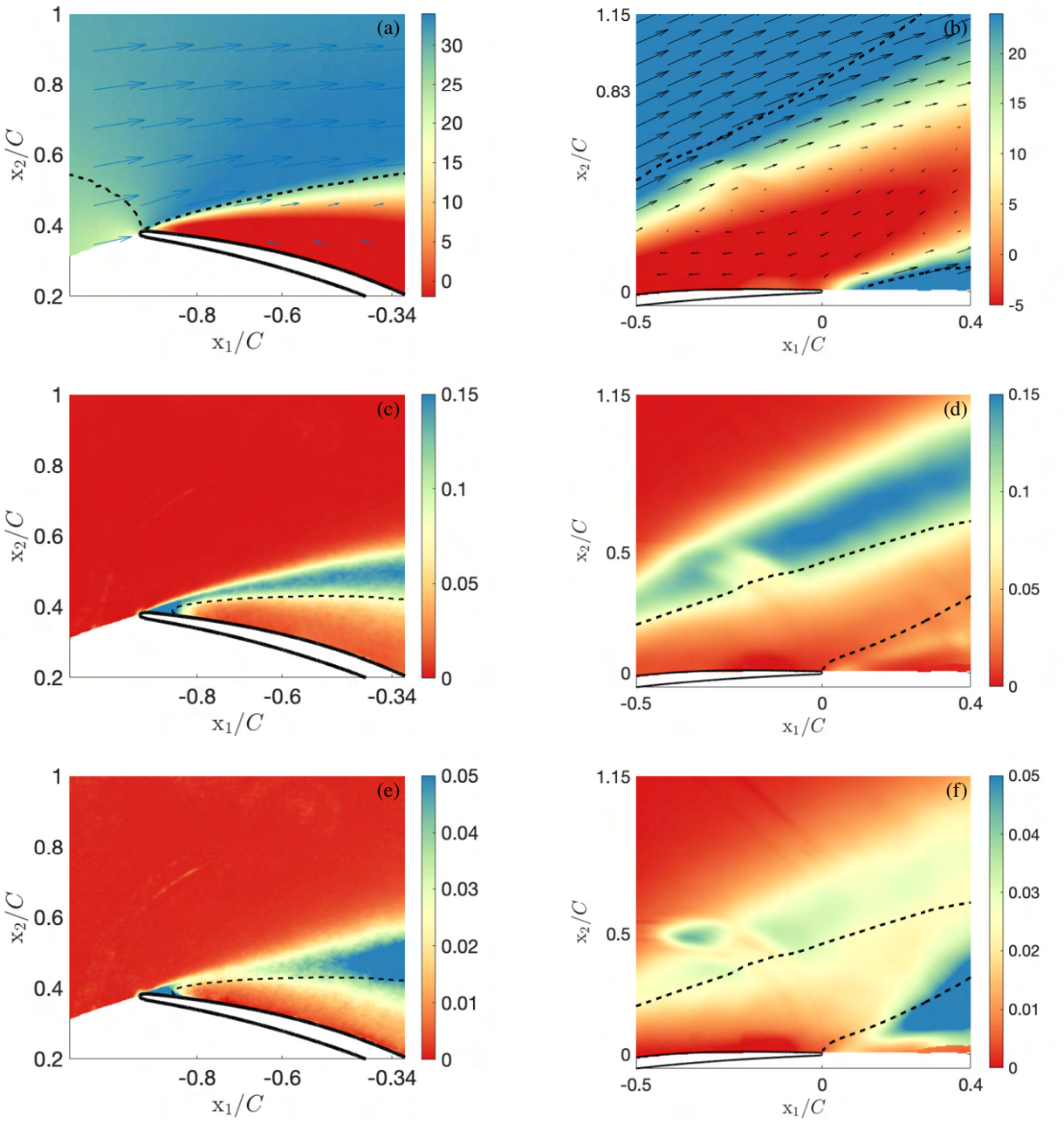

Fig. 6 Velocity statistics for α_g = 22° at 28 m/s. Flow is from left to right. Dotted black line are iso-countours of free-stream inlet velocity in figures (a) & (b) while they represent extent of the separation bubble in the subplots. Legends: (a) & (b) Mean streamwise velocity; (c) & (d) Streamwise velocity stresses $\frac{\overline{u_1 u_1}}{U_\infty^2}$; (e) & (f) Transverse velocity stresses $\frac{\overline{u_2 u_2}}{U_\infty^2}$.

A. Proper Orthogonal Decomposition

In order to identify the various modes of flow for an airfoil placed at high angles of attack, the Proper Orthogonal Decomposition (POD) technique as described by Holmes et al. [26] is used. The technique involves the decomposition of a dataset into a set of orthogonal basis functions, each of which captures a different mode or pattern in the data. These basis functions, known as eigenvalues, are ordered according to their energy. As such, POD allows identifying the underlying structures or modes of a system without requiring prior knowledge of the system's governing equations.

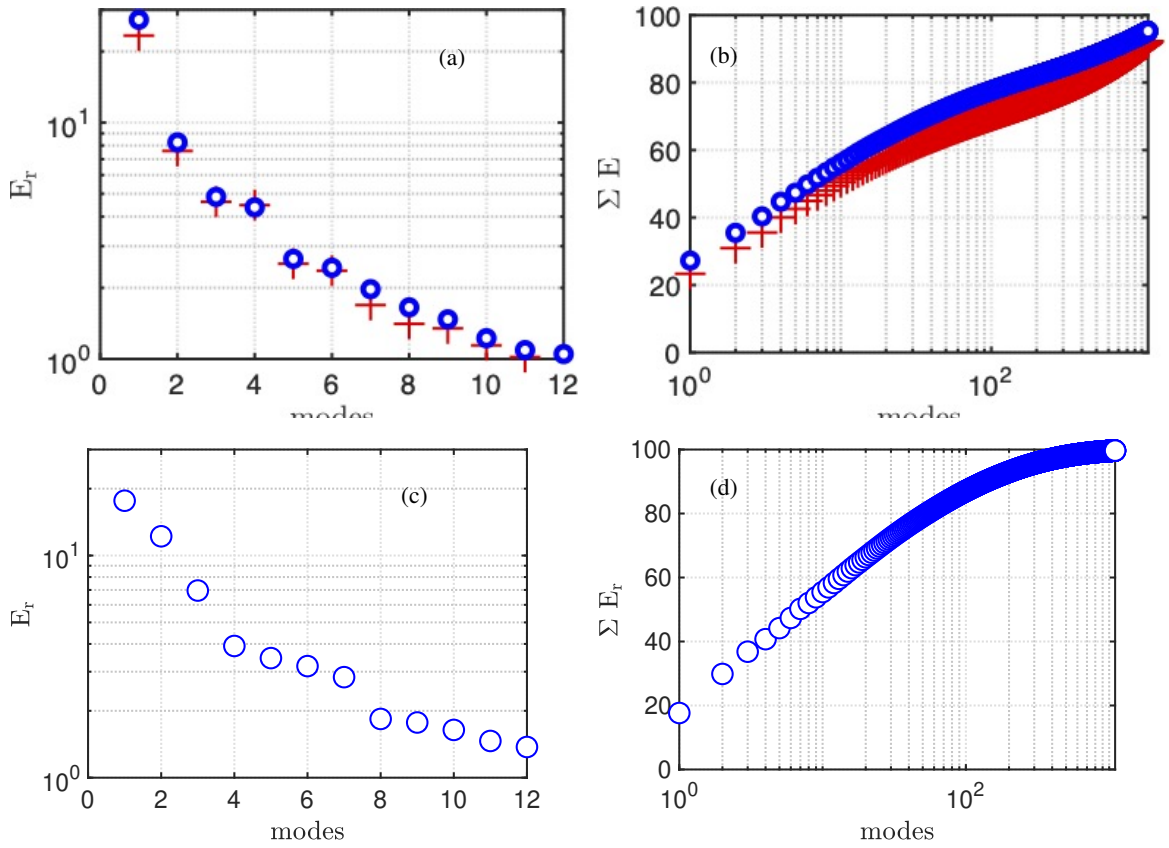

Fig. 7 POD based modal decomposition of the measured velocity field in the trailing-edge region (camera 3) for an airfoil placed at 15° angle of attack. (a) Relative energy of individual POD modes; (b) Cumulative sum of POD modes. Legends: Red cross for inlet velocity of U_∞ = 16 m/s while the blue circles represent inlet velocity of U_∞ = 28 m/s.

Instead, the POD relies on the data itself to reveal the dominant modes of motion or flow patterns.

In the present study the POD modes have been calculated using the Planar PIV data over the trailing-edge of the airfoil. The individual (E_r) and cumulative (ΣE) energy of mode distribution are shown in Fig. 7 for two angles of attack, α_g = 15° and α_g = 22° and two different inlet velocities. From Fig. 7 (b), it is clear that the cumulative energy for the higher flow velocity grows at a slightly faster rate. A one to one comparison cannot be made between Figs. 7 (b) and (d) because of differences in the field of view and spatial resolution achieved. While the modal pairs 3-4 and 5-6 appear to have similar energy for the α_g = 15°, they do not constitute an orthogonal convective basis [26]. In fact, no orthogonal convective modes were identified. In contrast Jaiswal et al. [22] had reported modal pairs associated to the passage of Kelvin-Helmholtz type flow instability, when the CD airfoil is placed at a much lower incidence. For such flows a frequency selection takes place for wavelengths that are associated with convective modes [22].

B. Far-field acoustic measurements

The far-field acoustic pressure is recorded by a single microphone, which is placed normal to the airfoil chord and at a distance of 1.21 m in the mid-span plane of the airfoil. The microphone signal is processed using the Welch's algorithm in order to calculate the Power Spectral Density (PSD). PSD is achieved with a spectral resolution of 1 Hz using a Blackman-Harris window, which minimizes the spectral leakage. The resulting PSD was normalised with reference pressure, i.e. 2×10^{-5} Pa in order to estimate the Sound Pressure Level (SPL), as shown in Fig. 8. These measurements were done for three different angles of attack at the same free stream velocity of 30 m/s. Fig. 8 clearly shows as the geometric angle of attack is increased from α_g = 8° to α_g = 15° the low-frequency (80-500 Hz) content of the SPL increases. However, with a further increase in geometric angle of attack (α_g = 22°), a reduction in the

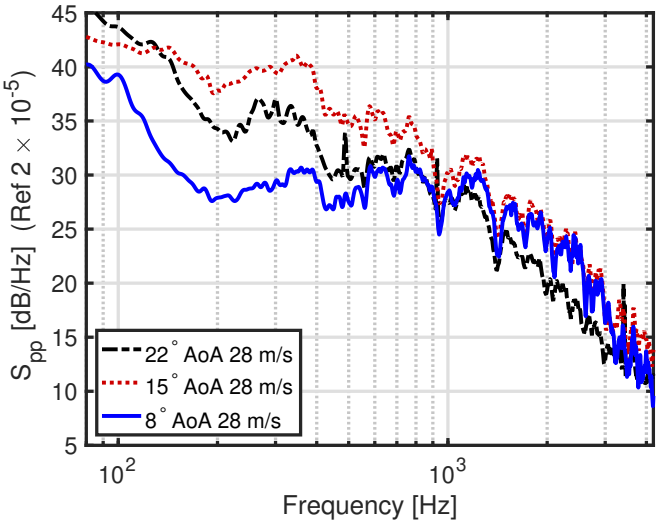

Fig. 8 Comparison of sound pressure level for various angles of attacks. Acoustic pressure measured at a distance of 1.21 **(m) in the mid-span plane.**

low-frequency content of the SPL can be seen compared to the $\alpha_g = 15°$. Therefore, SPL does not linearly increase for a given angle of attack despite a linear increase in boundary-layer thickness. Nevertheless, for the $\alpha_g = 22°$ case, the SPL remains high in the low-frequency region, however, a slight reduction is high-frequency part can be seen. These observations are consistent with the findings in [12]. Qualitatively, modulations in SPL associated with edge diffraction is substantially reduced for the case $\alpha_g = 22°$. Note that this edge diffraction is represented by Fresnel functions in Amiet [27]'s model. This most likely suggests that the noise sources are moving away from the wall and the edge in the case of deep stall, and that larger structures are contributing to the far-field sound and that the airfoil becomes more compact justifying the analytical model proposed by Moreau et al. [11] in that case.

IV. Discussion and conclusions

Separated and stalled flow-field characterization of the CD airfoil was performed using PIV. The present paper reports velocity field measurement at two angles of attacks and velocities. When the CD airfoil placed at $\alpha_g = 15°$, irrespective of the mean inlet velocity, the mean flow re-attaches at the trailing-edge region. However, as the angle of attack is increased further to $\alpha_g = 22°$, the airfoil experiences a deep stall, and the mean flow remains detached over the whole airfoil chord.

The low-frequency content of the airfoil self noise increases as the angle of attack is increased from 8° to 15°. This increased noise is also accompanied by an increase in the amplitude of wall-pressure and velocity disturbances. The genesis of the increased disturbances can be linked to the late transition of boundary layer. In particular, as the angle of attack is increased, the LSB was found to cover at least 40% of the airfoil chord consistently with previous LES results [28, 29], which leads to a delayed flow transition and re-attachment, somewhere between 40 and 65% of the chord length. As such, the magnitude of flow disturbances represented by the dimensionless Reynolds stress components $\overline{u_1u_1}/U_\infty^2$, $\overline{u_2u_2}/U_\infty^2$, and $-\overline{u_1u_2}/U_\infty^2$, increases substantially compared to airfoil at 8° attack, especially close to the airfoil trailing edge. Note that increasing the Reynolds number does not change the flow patterns substantially, but only decreases the levels of velocity fluctuations and Reynolds stresses near the trailing edge.

However, a further increase in the angle of attack leads to a decrease in the SPL. As such, the increase in the low-frequency noise is accompanied by an increase in the amplitude in the velocity disturbances levels. Consequently the SPL does not scale with the boundary-layer thickness as has been conjectured by [16]. This is because the near-field disturbances, which are the source of term for trailing-edge noise [21], does not scale the boundary-layer or the shear layer thickness. As such, a one to one relation does not exists between SPL and boundary layer thickness (or shear layer thickness) for an airfoil undergoing deep stall.

V. Acknowledgements

The authors acknowledge the support of the Natural Sciences and Engineering Research Council of Canada (NSERC) through the Discovery grant.

References

[1] Arroyo, C. P., Kholodov, P., Sanjosé, M., and Moreau, S., "CFD modeling of a realistic turbofan blade for noise prediction. Part 1: Aerodynamics," *Proceedings of the Global Power and Propulsion Society (GPPS, 2019)*, 2019.

[2] Koch, R., Sanjose, M., and Moreau, S., "Numerical investigation of noise sources in a single airfoil tip-leakage flow," *25th AIAA/CEAS Aeroacoustics Conference*, 2019, p. 2625.

[3] Perennes, S., and Roger, M., "Aerodynamic noise of a two-dimensional wing with high-lift devices," *4th AIAA/CEAS aeroacoustics conference*, Toulouse,France, 1998, p. 2338.

[4] Manoha, E., Bulté, J., and Caruelle, B., "LAGOON: an experimental database for the validation of CFD/CAA methods for landing gear noise prediction," *14th AIAA/CEAS aeroacoustics conference (29th AIAA aeroacoustics conference)*, Vancouver, British Columbia, Canada, 2008, p. 2816.

[5] Lacagnina, G., Chaitanya, P., Berk, T., Kim, J., Joseph, P., Ganapathisubramani, B., Hasheminejad, S., Chong, T., Stalnov, O., Choi, K., et al., "Investigation on the mechanism for the aerofoil noise near stall conditions," *Physical Review Fluids*, 2019.

[6] Paterson, R. W., Amiet, R. K., and Munch, C. L., "Isolated airfoil-tip vortex interaction noise," *Journal of Aircraft*, Vol. 12, No. 1, 1975, pp. 34–40.

[7] Lakshminarayana, B., *Fluid Dynamics and Heat Transfer of Turbomachinery*, John Wiley & Sons, Inc., 1996.

[8] Crevel, F., Gourdain, N., and Moreau, S., "Numerical simulation of aerodynamic instabilities in a multistage high-speed high-pressure compressor on its test-rig : part 1 - Rotating stall," *Journal of Turbomachinery*, Vol. 136, No. 10, 2014, pp. 101003–1–14.

[9] Christophe, J., and Moreau, S., "LES of the trailing-edge flow and noise of a controlled-diffusion airfoil at high angle of attack," *Proceedings of the Summer Program*, Stanford, California, U.S.A, 2008, p. 305.

[10] Mayer, Y., Zang, B., and Azarpeyvand, M., "Aeroacoustic characteristics of a NACA 0012 airfoil for attached and stalled flow conditions," *25th AIAA/CEAS Aeroacoustics Conference*, Delft, The Netherlands, 2019, p. 2530.

[11] Moreau, S., Roger, M., and Christophe, J., "Flow features and self-noise of airfoils near stall or in stall," *15th AIAA/CEAS Aeroacoustics Conference (30th AIAA Aeroacoustics Conference)*, Miami, Florida, 2009, p. 3198.

[12] Kalyani, S. K., Moreau, S., and Ragni, D., "Flow-field and Noise Characterization of a Controlled-Diffusion Airfoil," *28th AIAA/CEAS Aeroacoustics 2022 Conference*, 2022, p. 2894.

[13] Christophe, J., Anthoine, J., and Moreau, S., "Trailing edge noise computation of a fan blade profile," *The Journal of the Acoustical Society of America*, Vol. 123, No. 5, 2008, pp. 3539–3539.

[14] Kholodov, P., and Moreau, S., "Identification of noise sources in a realistic turbofan rotor using Large Eddy Simulation," *Acoustics*, Vol. 2, Multidisciplinary Digital Publishing Institute, 2020, pp. 691–706.

[15] Caro, S., and Moreau, S., "Aeroacoustic modelling of low pressure axial flow fans," *6th Aeroacoustics Conference and Exhibit*, Lahaina,HI,U.S.A., 2000, p. 2094.

[16] Brooks, T. F., and Hodgson, T. H., "Trailing edge noise prediction from measured surface pressures," *Journal of sound and vibration*, Vol. 78, No. 1, 1981, pp. 69–117.

[17] Padois, T., Laffay, P., Idier, A., and Moreau, S., "Detailed experimental investigation of the aeroacoustic field around a Controlled-Diffusion airfoil," *21st AIAA/CEAS aeroacoustics conference*, Dallas, TX, U.S.A., 2015, p. 2205.

[18] Moreau, S., and Roger, M., "Effect of airfoil aerodynamic loading on trailing edge noise sources," *AIAA journal*, Vol. 43, No. 1, 2005, pp. 41–52.

[19] Neal, D., "Effects of rotation on the flow field over a Controlled-Diffusion airfoil," Ph.D. thesis, Michigan, 2010.

[20] Wu, H., Laffay, P., Idier, A., Jaiswal, P., Sanjosé, M., and Moreau, S., "Numerical study of the installed controlled diffusion airfoil at transitional Reynolds number," *Mathematical and Computational Approaches in Advancing Modern Science and Engineering*, Springer, 2016, pp. 505–515.

[21] Ffowcs Williams, J. E., and Hall, L. H., "Aerodynamic sound generation by turbulent flow in the vicinity of a scattering half plane," *Journal of fluid mechanics*, Vol. 40, No. 4, 1970, pp. 657–670.

[22] Jaiswal, P., Pasco, Y., Yakhina, G., and Moreau, S., "Experimental investigation of aerofoil tonal noise at low Mach number," *Journal of Fluid Mechanics*, Vol. 932, 2022, p. A37.

[23] Moreau, S., Christophe, J., and Roger, M., "LES of the trailing-edge flow and noise of a NACA0012 airfoil near stall," *Proceedings of the Summer Program*, Stanford University, Center for Turbulence Research Stanford, CA, USA, 2008, pp. 317–329.

[24] Medjnoun, T., "Experimental investigation of secondary flows in turbulent boundary layers," Ph.D. thesis, University of Southampton, 2020.

[25] McLaughlin, B., Lawson, J., and Ganapathisubramani, B., "Measuring Instantaneous Forces with a Photoelastic Force Balance," *AIAA SCITECH 2023 Forum*, 2023, p. 1937.

[26] Holmes, P., Lumley, J. L., Berkooz, G., and Rowley, C. W., *Turbulence, coherent structures, dynamical systems and symmetry*, Cambridge university press, 2012.

[27] Amiet, R. K., "Noise due to turbulent flow past a trailing edge," *Journal of sound and vibration*, Vol. 47, No. 3, 1976, pp. 387–393.

[28] Christophe, J., Anthoine, J., and Moreau, S., "Trailing edge noise of a controlled-diffusion airfoil at moderate and high angle of attack," *15th AIAA/CEAS Aeroacoustics Conference (30th AIAA Aeroacoustics Conference)*, Miami, Florida, 2009, p. 3196.

[29] Christophe, J., "Application of Hybrid Methods to High Frequency Aeroacoustics," Ph.D. thesis, von Karman Institute for Fluid Dynamics / Universite Libre de Bruxelles, 2011.